RSC Advances

PAPER

View Article Online
View Journal | View Issue

Cite this: RSC Adv., 2016, 6, 77284

Tuning magnetoresistive and magnetocaloric properties *via* grain boundaries engineering in granular manganites

Abd El-Moez A. Mohamed,*[ab] Mohamed A. Mohamed,[c] V. Vega,[b] B. Hernando[b] and A. M. Ahmed[a]

In this work, we investigate the effect of interface size on the electrical, magnetoresistive, magnetic and magnetocaloric properties of the $La_{0.7}Ba_{0.3}MnO_3$ (LBMO) manganite compound. This is done by introducing different sizes of secondary phases of Ni and Ag (Ni powder, Ni nanowires, Ag oxide powder and Ag nanoparticles) to the LBMO compound, forming inhomogeneous systems of LBMO/Ni and LBMO/Ag composites. X-Ray diffraction patterns reveal the interaction lack between Ni & Ag interfaces and LBMO compound through the coexistence of their characteristic peaks. This suggests the segregation of these interfaces between LBMO grains, leading to a change in the boundary resistance that is found to be an interface-size-dependent change. Accordingly, the transport properties of LBMO are changed, where, the resistivity increases and the metal–semiconductor transition temperature decreases with the introduced interfaces. The change in grain boundary resistance enhances the magnetoresistive properties during the promotion of the spin carrier tunnelling process. For instance, the room temperature low field magnetoresistance of the LBMO compound is enhanced from −1.23% to −4.35, −5.25 and −7.9% with the introduction of Ni powder, Ag nanoparticles and Ag oxide powder interfaces, respectively. The dc thermal magnetization measurements show a constant value of the LBMO Curie temperature (T_c) with the introduced interfaces that may be attributed to the complete interaction lack. However, a small decrease is registered in the T_c value of Ni nanowires doped LBMO composite, that may be due to the incomplete interaction lack in this composite. Moreover, the magnetocaloric properties of the LBMO compound show a notable enhancement with the introduced interfaces, where its relative cooling power is enhanced from 44 J kg^{-1} to 107, 167, 92 and 94 J kg^{-1} with the introduction of Ni powder, Ni nanowires, Ag oxide and Ag nanoparticle interfaces, respectively, at a 3 T applied magnetic field.

Received 18th June 2016
Accepted 27th July 2016

DOI: 10.1039/c6ra15874a

www.rsc.org/advances

1. Introduction

Numerous works have discussed the appearance of low field magnetoresistance (LFMR) in defected manganites. Principally, defects interrupt conduction between grains, so, carriers resort to tunnelling process across grain boundaries (GBs) that result in the LFMR effect.[1] GBs are natural defects, whose effect increases in the small grain size systems. This fact has increased the interest in granular systems and has encouraged the promotion of artificial granularity. For example, granularity can be increased by the introduction of interfaces or secondary phases with ferromagnetic materials.[2] These inhomogeneous systems have been studied in manganites as $La_{0.7}Sr_{0.3}MnO_3$/ZrO_2 (ref. 3) and $La_{0.67}Ca_{0.33}MnO_3$/ZnO,[4] which have shown a good LFMR promotion. In fact, the high values of LFMR are observed below the T_c due to the extrinsic nature of this type of MR. However, the room temperature LFMR values are still suitable for some technological applications.[5] Besides the magnetoresistive properties, manganites have shown a high magnetic entropy change (ΔS) around T_c under the effect of magnetic field application, which makes them remarkable magnetocalorics for magnetic cooling technologies.[6] Actually, the most remarkable feature of the inhomogeneous granular manganite/secondary phase systems is the interaction lack between their contents. Due to this interaction lack, the secondary phase is expected to be segregated among the manganite material grains. This increases the GBs' resistance leading to the LFMR effect. This view point has been supported in several experimental works as in $La_{0.66}Ca_{0.33}MnO_3$/$SrTiO_3$,[7] $La_{0.67}Ba_{0.33}MnO_3$/YSZ[8] and $La_{0.66}Sr_{0.33}MnO_3$/CeO_2.[9] Moreover, the complete interaction lack retains the intrinsic properties of the manganite material without any change, such as the T_c

[a]Physics Department, Faculty of Science, Sohag University, Sohag 82524, Egypt. E-mail: abdmoez_hussien@science.sohag.edu.eg

[b]Physics Department, Faculty of Science, Oviedo University, Oviedo 33007, Spain

[c]Instituto de Biología Molecular y Celular de Plantas, Consejo Superior de Investigaciones Científicas-Universidad Politécnica de Valencia, Valencia 46022, Spain

value. Thus, the T_c related phenomena as the magnetocaloric effect (MCE) can be tuned at the same working temperature range (around T_c). Making use of the interaction lack feature, we studied previously the secondary phase ratio effect on the magnetoresistance and the MCE of LBMO manganite in the LBMO/xTiO$_2$ system.[10] These results showed a notable enhancement in the LFMR and the MCE of LBMO manganite with increasing TiO$_2$ ratio. Due to the GBs' resistance-dependence on the secondary phase distribution at GBs, we also studied the effect of annealing temperature on TiO$_2$ distribution among LBMO grains.[11] It was found that the high MCE efficiency in these granular systems can be obtained at higher annealing temperatures. Accordingly, after the impact on GBs' resistance of the interface ratio and interface distribution is studied, it is interesting to complete this investigation by studying the effect of interface size on GBs' resistance and related properties. This is done by introducing different sizes of Ni and Ag interfaces to the ferromagnetic LBMO manganite compound. In this case we can study the sensitivity of GBs' resistance to the interface size and its effect on transport, magnetic, LFMR and MCE properties of the LBMO compound.

2. Experimental

LBMO/M$_{0.02}$ composites were prepared in several steps, M is elemental Ni powder (Ni$_{powder}$), Ni nanowires (Ni$_{NWs}$), Ag oxide (Ag$_{oxide}$) and Ag nanoparticles (Ag$_{NPs}$). First, the LBMO compound was prepared by the sol–gel method, as reported in ref. 10. Ni element and Ag oxide powder are commercial and used as provided. Ni$_{NWs}$ were prepared by the pulsed electrochemical deposition (PED) method, as in ref. 12, and Ag$_{NPs}$ were prepared as reported in ref. 13. Second, stoichiometric amounts of LBMO, Ni$_{powder}$, Ni$_{NWs}$, Ag$_{oxide}$ and Ag$_{NPs}$ were mixed, pelletized and annealed at 800 °C for 24 hours. The crystal structure was examined by X-ray diffraction (XRD) technique at room temperature and the surface morphology was investigated by a scanning electron microscope (SEM); structural analysis was carried out with Rietveld analysis using the FULLPROF program. Electrical resistivity was measured with the standard four-point Van der Pauw technique and magnetic properties were carried out using a vibrating sample magnetometer (VSM).

3. Results and discussion

3.1 Structure

The XRD patterns in Fig. 1 show the high phase purity of the LBMO compound with extra peaks in the doped composites that belong to Ni and Ag interfaces. The existence of these extra peaks in doped composites reveals their interaction lack with the LBMO compound. This suggests interfaces segregation on the surfaces and between the boundaries of LBMO grains, which is confirmed by the SEM micrographs in Fig. 2. The interface–LBMO interaction lack leads to the stability of structural properties in all composites as: (I) the $R\bar{3}c$ rhombohedral structure; and (II) the insignificant change in the cell volume, the average SEM grain size and the average crystallite size (P) (that was calculated from the Laue–Scherrer equation) as displayed in Table 1, Rietveld profiles are presented in Fig. 1c and d. The observed large difference between the crystallite size and the SEM grain size suggests crystallite collectivisation inside the grains due to structural defects and/or internal stresses.[14] It is noteworthy to state that the XRD analysis exhibits the presence of NiO in the LBMO/Ni$_{powder}$ composite instead of Ni element, which may be oxidized through the annealing process. Also, we observe the higher intensity of the Ni peak in the LBMO/Ni$_{powder}$ composite in comparison with that in the LBMO/Ni$_{NWs}$ composite. This difference in peak intensity may be attributed to the smaller size of Ni NWs that enables some of them to interact substitutionally with the Mn ions in the LBMO compound, decreasing the segregated amount and leading to the smaller Ni peak intensity in the LBMO/Ni$_{NWs}$ composite. In contrast, the similar Ag peak intensity in both Ag-doped LBMO composites (oxide and NPs) reveals the complete interaction lack between the Ag interfaces and the LBMO compound.

3.2 Transport properties

The temperature dependence of zero magnetic field resistivity in Fig. 3 shows the metal–semiconductor transition for all composites at the T_{ms} temperature, where the T_{ms} arises from the ferromagnetic double exchange (DE) interaction (Mn^{3+}–O–Mn^{4+}).[15] The presence of Ni and Ag interfaces increases LBMO resistivity and shifts its T_{ms} towards lower temperatures (see Table 2), in agreement with the results in ref. 3, 4 and 8. Due to the interface–LBMO interaction, the change in LBMO transport properties with the introduced interfaces is suggested to have

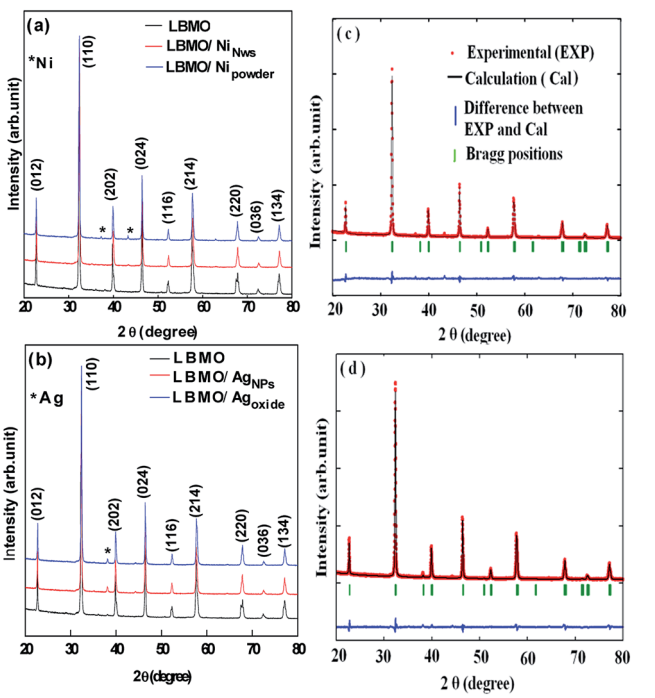

Fig. 1 (a) and (b) XRD patterns of LBMO/Ni and LBMO/Ag doped composites, respectively, and (c) and (d) Rietveld profiles for LBMO/Ni$_{powder}$ and LBMO/Ag$_{oxide}$ composites, respectively.

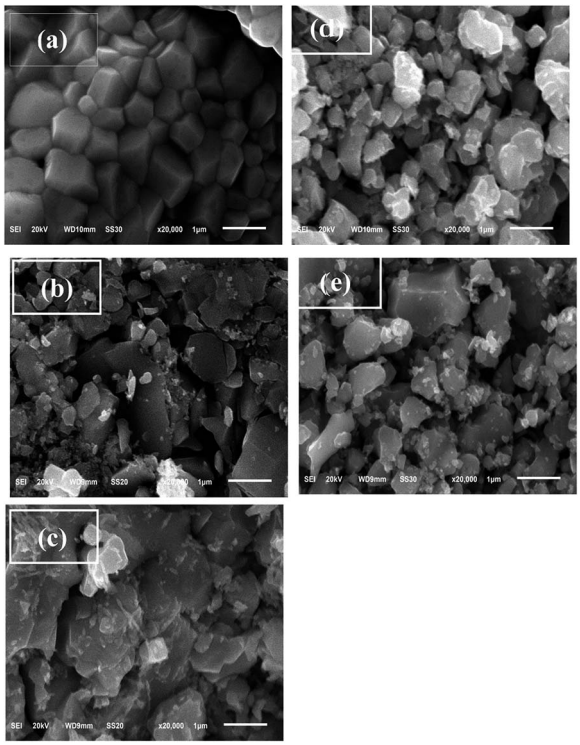

Fig. 2 SEM micrographs for LBMO doped composites, where, (a) LBMO, (b) LBMO/Ni_{powder}, (c) LBMO/Ni_{NWs}, (d) LBMO/Ag_{oxide}, and (e) LBMO/Ag_{NPs} doped composites, respectively.

an extrinsic origin, which comes from the GBs effect. In other words, the presence of such interfaces between LBMO grains increases their boundary resistance[8,10,11] promoting carrier scattering and increasing the resistivity. The situation can be visualized as an interruption in the direct contact between LBMO grains through the increase in their boundaries thickness due to interfaces accumulation.[16] The change in GBs' resistance with the introduced interfaces can be experimentally realized through the low temperature resistivity increase ($\rho_{100\ K}$), see Table 2, which mainly arises from the GB effect.[2,10] Fig. 3 also shows the LBMO resistivity dependence on the interface size, which reveals the GBs' sensitivity to the introduced size. For example, the LBMO/Ag_{NPs} compound shows a smaller resistivity and a higher T_{ms} value than the LBMO/Ag_{oxide}.

This is because of the different interface distributions at the GBs according to their sizes, which results in different changes in the GBs' resistance.[11] SEM micrographs in Fig. 2 show the well agglomeration of the smaller size interfaces (Ni NWs and

Table 1 Phase symmetry, cell volume (V), the average SEM grain size (G) and the average crystallite size (P) for LBMO doped composites

Compound	Symmetry	V/Å^3	G/μm	P/nm
LBMO[10]	$R\bar{3}c$ rhombohedral	358.8	0.748	32
LBMO/Ni_{powder}	$R\bar{3}c$ rhombohedral	358.5	0.70	35
LBMO/Ni_{NW}	$R\bar{3}c$ rhombohedral	357.0	0.65	34.7
LBMO/Ag_{oxide}	$R\bar{3}c$ rhombohedral	358.4	0.72	35.7
LBMO/Ag_{NP}	$R\bar{3}c$ rhombohedral	358.4	0.75	35.4

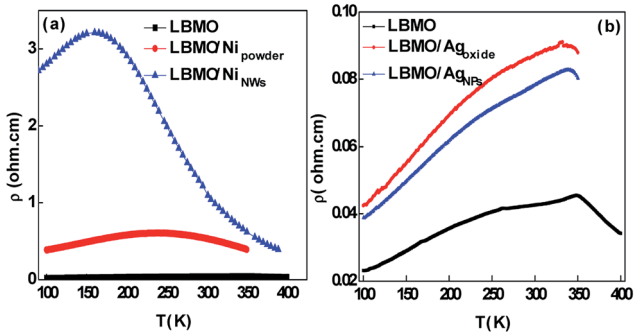

Fig. 3 The temperature dependence of resistivity for (a) LBMO/Ni and (b) LBMO/Ag composites, respectively.

Ag NPs) away from boundaries, which leads to a small effect on the GBs' resistance in these doped composites. This can be inferred through the smaller value of $\rho_{100\ K}$ of LBMO/Ag_{NPs} in comparison with that of LBMO/Ag_{oxide} composites (see Table 2). However, Ni-doped composites does not obey this scenario; the LBMO/Ni_{NWs} composite shows a higher resistivity and a smaller T_{ms} value than the LBMO/Ni_{powder} composite in spite of the well agglomerated Ni NWs away from the GBs. This is because the proposed scenario works only with resistivity arising from extrinsic factors (*e.g.* the change in GBs resistance), while in the LBMO/Ni_{NWs} composite, there is an additional intrinsic resistance component (ρ_{int}). This ρ_{int} arises from the small partial substitution of Mn by Ni that forms Mn–O–Ni bonds and suppresses the ferromagnetic DE interaction (Mn^{3+}–O–Mn^{4+}). Mn–O–Ni bonds are non double exchangeable interactions with an antiferromagnetic nature and result in a stronger localization in the e_g electron, which explains the notable increase in the resistivity of this doped composite, as seen in Fig. 3.

Fig. 4 shows the temperature dependence of MR, where, it was determined through the equation MR = $(\rho_H - \rho_0)/\rho_0$, ρ_0 and ρ_H are resistivities in 0 T and 0.5 T applied magnetic fields, respectively. The negative MR characterizes all composites over whole the temperature range except for the LBMO/Ni_{NWs} composite, which shows a crossover from negative to positive MR at a certain temperature. The LBMO compound shows a MR peak near T_c with a maximum value of −3%. The MR of LBMO is enhanced in all doped composites across the temperature range (except for the LBMO/Ni_{NWs} composite), and the MR peak is shifted towards room temperature with an improvement of −3.7, −4.9 and −8.2% for Ni_{powder}, Ag_{NPs} and Ag_{oxide} interfaces,

Table 2 Transport, magnetoresistive, magnetic and magnetocaloric parameters for LBMO/Ni and LBMO/Ag systems

Compound	T_{ms}/K	T_c/K	$\rho_{100\ K}$/Ω cm	$MR_{300\ K}$ (%)	δT_{FWHM}/K	RCP/J kg^{-1}
LBMO[10]	350	348	0.023	−1.23	24	44
LBMO/Ni_{powder}	240	348	0.38	−4.35	70	107
LBMO/Ni_{NWs}	160	342	2.8	8.05	106.7	167
LBMO/Ag_{oxide}	332	348	0.042	−7.9	57.37	92
LBMO/Ag_{NPs}	338	348	0.038	−5.25	58.63	94

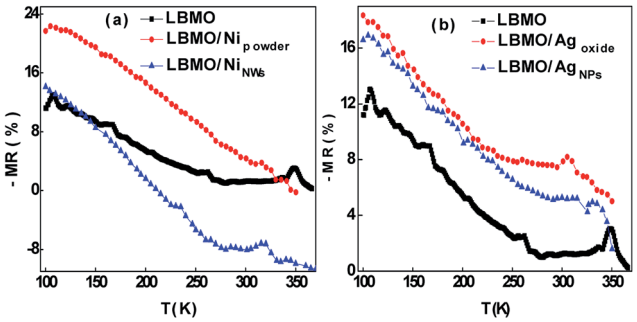

Fig. 4 The temperature dependence of MR for (a) LBMO/Ni and (b) LBMO/Ag composites, respectively.

respectively, in agreement with ref. 17–19. The promotion in LFMR includes the room temperature values (300 K) as displayed in Table 2. The enhanced LFMR with the introduced interfaces refers to the spin polarized tunnelling process between grains due to the increase in GB resistance.[1,20] The results of LFMR show an interface size dependent behaviour, in which the high values of LFMR can be observed at the higher interface size as seen in Fig. 4. This is because of the spin tunnelling process dependence on the GBs' thickness, which in turn increases with the interface size.

The anomalous behaviour of the MR sign change in the LBMO/Ni_{NWs} composite can be explained according to the spin carriers near the Fermi level (E_F). In general, negative and positive MR arise from majority and minority spin carriers near the Fermi level (E_F), respectively.[21] Accordingly, a spin carrier change is suggested in the Ni NWs-doped composite. In the LBMO compound, Ba^{2+} electrons remain at the e_g band of the Mn ion acting as a major spin carrier near E_F, which is the negative MR case. This case is preserved in the Ni powder and in both Ag-doped composites due to the complete interaction lack. Meanwhile, due to the partial substitution process in the LBMO/Ni_{NWs} composite, at low temperatures Ni electrons also occupy the e_g band of the Mn ion, keeping the majority spin carriers near E_F and the negative MR. However, during temperature elevation, Ni electrons no longer stay in the e_g band and instead migrate to the $t_{2g}^{\downarrow}$ band whose edge is quite closer to the E_F than the e_g band. The occupation of the $t_{2g}^{\downarrow}$ band by Ni electrons causes these Mn ions to adopt in an antiparallel alignment with the system being as minority spin carriers near the E_F that leads to the positive MR.[21]

3.3 Magnetic properties

Fig. 5 displays the temperature dependence of magnetization curves, $M(T)$, at 100 Oe applied magnetic field for Ni and Ag doped composites. The Figure shows the ferromagnetic–paramagnetic (FM–PM) transition for all composites at T_c. Two important features can be drawn from this Figure. The first is the constant value of the LBMO compound T_c at 348 K with the introduced Ni_{powder} and both Ag interfaces (see Table 2), in agreement with results in ref. 10, 22 and 23. The constant T_c value is due to its intrinsic character and its dependence on the grain's internal ferromagnetism, which remains unchanged due to the complete interaction lack in these composites. Meanwhile, the incomplete interaction lack in the LBMO/Ni_{NWs} composite decreases the T_c value to 342 K as a result of the partial substitution process of the Mn ion, which suppresses

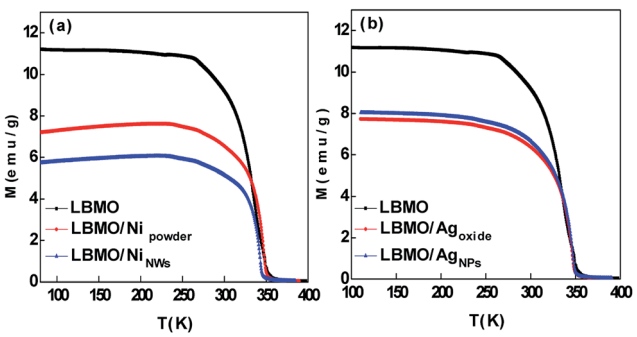

Fig. 5 Thermal dependence of dc magnetization at 100 Oe applied magnetic field for (a) LBMO/Ni and (b) LBMO/Ag composites, respectively.

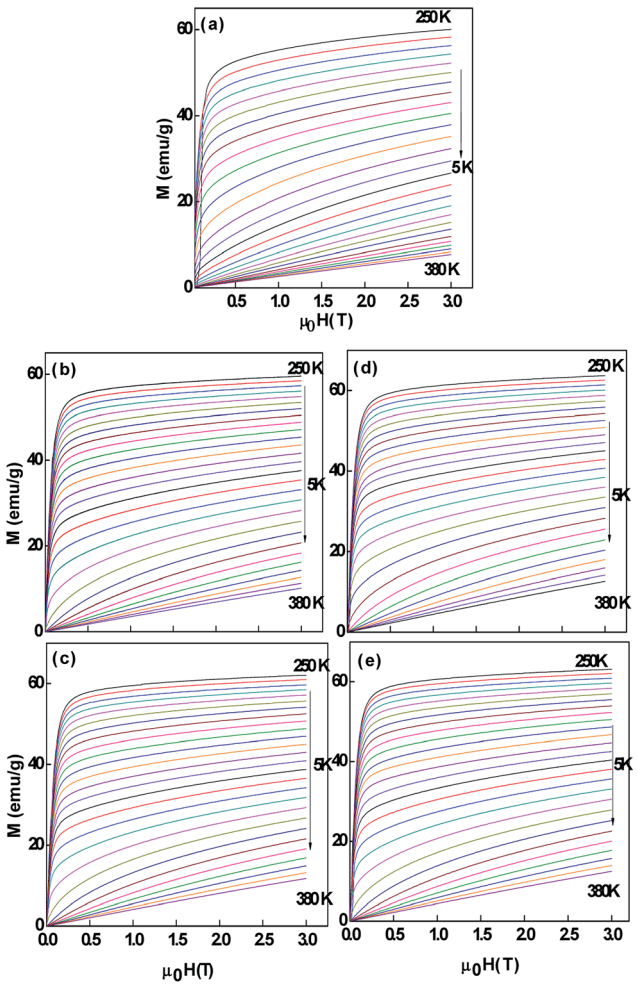

Fig. 6 Isothermal magnetization curves of (a) LBMO, (b) LBMO/Ni_{powder}, (c) LBMO/Ni_{NWs}, (d) LBMO/Ag_{oxide} and (e) LBMO/Ag_{NPs} doped composites.

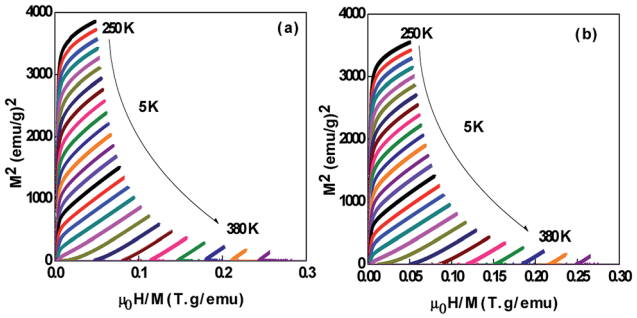

Fig. 7 Arrott plots for (a) LBMO/Ni_{NWs} and (b) LBMO/Ni_{powder} doped composites as selected examples.

ferromagnetism due to the formation of Mn–O–Ni antiferromagnetic bonds. The second note is concerned with the change in magnetization value, where the magnetization of LBMO compound decreases with interfaces introduction. The interaction lack in doped composites excludes the role of intrinsic factors in the magnetization change and instead shows the GBs' role.[11,23] In principle, we can say that the ferromagnetism inside LBMO grains is interrupted and pinned by GBs, and both Ni and Ag interfaces increase the GBs' thickness and resistance, leading to ferromagnetism pinning and confinement inside the grains. This explains the decrease in LBMO magnetization with interfaces introduction. Moreover, it is noteworthy that the magnetization dependence on the interface size,[11] which may be attributed to the GBs resistance senistivity to the interface size. This is because the low GB resistance reduces pinning effect, therefore, the smaller interface size the higher magnetization value in the doped composites, and *vice versa*. This is clearly seen in both LBMO/Ag composites, where, the LBMO/Ag_{NPs} composite shows a magnetization value higher than the LBMO/Ag_{oxide} composite. Again, this explanation may not be convenient for Ni-doped composites, since, the LBMO/Ni_{powder} composite shows a magnetization value greater than the LBMO/Ni_{NWs} composite. The reason for this anomalous behaviour involves also the intrinsic effects, which are added to the extrinsic ones due to the small Mn partial substitution process in the LBMO/Ni_{NWs} composite. As a consequence, the magnetization change in this composite is a sum of two components; an extrinsic one coming from magnetization pinning by GBs and the other from ferromagnetism suppression due to the Mn–O–Ni antiferromagnetic bonds.

The isothermal magnetization curves in Fig. 6 show the FM–PM transition. The FM behaviour appears in curves below T_c as a sharp increase in magnetization with low applied magnetic fields followed by saturation at high fields. Meanwhile, the paramagnetic behaviour characterizes curves above T_c, where the magnetization changes linearly with the applied magnetic field. Arrott plots[24] in Fig. 7 prove the second order nature of this magnetic transition for all composites due to the positive slope around T_c.[25] This reveals the non-impact of the LBMO magnetic transition type by the introduced interfaces.

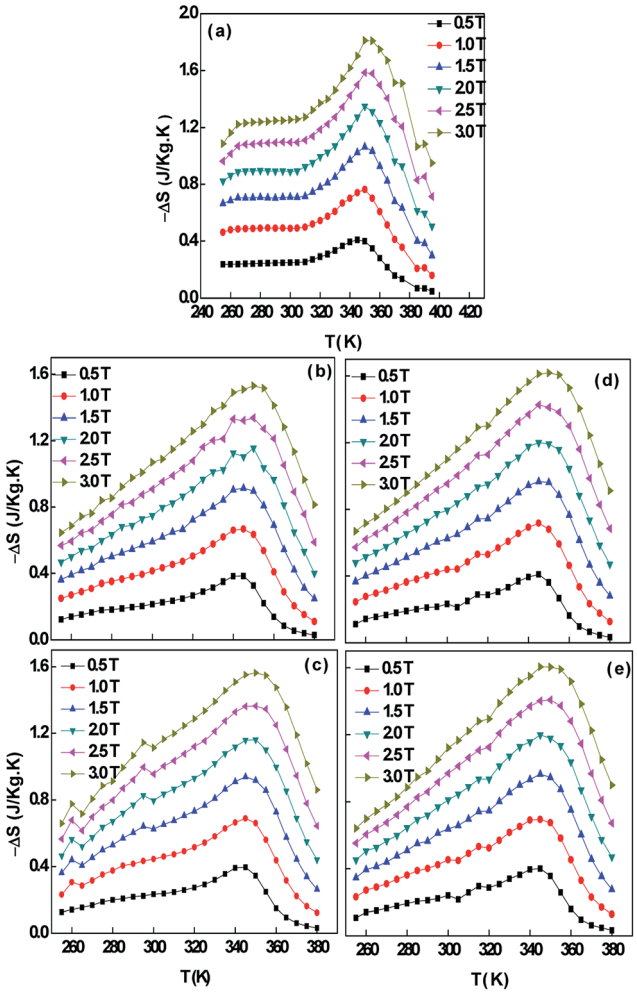

Fig. 8 The temperature dependence of ΔS at different applied magnetic fields for (a) LBMO, (b) LBMO/Ni_{powder}, (c) LBMO/Ni_{NWs}, (d) LBMO/Ag_{oxide} and (e) LBMO/Ag_{NPs} doped composites.

3.4 Magnetocaloric effect (MCE)

$$\Delta S(T, \Delta H) = \sum (M_i - M_{i+1})/(T_i - T_{i+1})\Delta H \quad (1)$$

$$\mathrm{RCP} = \Delta S_{max} \times \delta T_{FWHM} \quad (2)$$

ΔS was calculated from the isothermal magnetization curves using the approximated Maxwell relation in eqn (1),[26] where M_{i+1} and M_i are magnetization values measured at temperatures T_{i+1} and T_i in a magnetic field change ΔH. The temperature dependence of ΔS displayed in Fig. 8 shows a maximum (ΔS_{max}) around T_c, which increases monotonically with the applied magnetic field. In spite of the negligible change in the ΔS_{max} value of LBMO with the introduced Ni and Ag interfaces, there is no registered change in the temperature position, which means no change in the working temperature range (around the same T_c value). The stability in the working temperature range refers to the preservation of intrinsic properties due to the interaction lack. ΔS has a strong correlation with the ferromagnetic

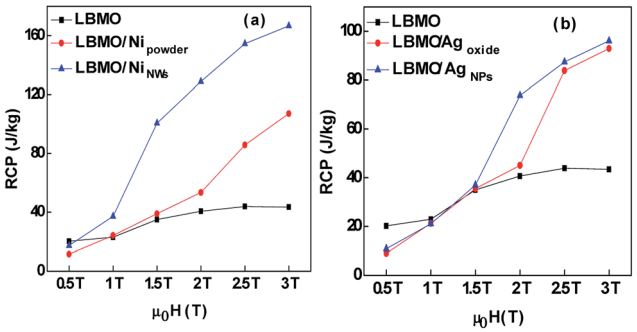

Fig. 9 Magnetic field dependence of RCP for (a) LBMO/Ni and (b) LBMO/Ag doped composites.

intrinsic Mn^{3+}/Mn^{4+} DE interaction and the T_c, which are kept without any change. In spite of the negligible change in the ΔS_{max} value of LBMO with the Ni and Ag interfaces, a promising feature related to the width of $\Delta S(T)$ curve can be observed, which can be expressed in terms of the full width at half maximum (δT_{FWHM}). Results in Table 2 show the enhancement in the δT_{FWHM} value of the LBMO compound with the introduction of interfaces, which means an increase in the MCE working temperature range, in agreement with results of LBMO/TiO_2.[10] The relative cooling power (RCP) is one of concepts that reflect the MCE efficiency, where it expresses the transferred heat between hot and cold reservoirs in one thermodynamic cycle.[27] The RCP values have been calculated using eqn (2) and the results are displayed in Fig. 9. This Figure shows the notable enhancement in the RCP values of the LBMO compound with Ni and Ag interfaces at applied magnetic fields ≥1.5 T. Also, we note a greater enhancement in the smaller-size-interface doped composites in comparison with the larger interface sizes, in agreement with M. Pekala *et al.*[28] For example, as seen in Table 2, the RCP value of the LBMO compound is improved from 44 J kg^{-1} to 107 & 167 J kg^{-1} in composites with Ni powder and Ni NWs interfaces, respectively, and to 92 & 94 J kg^{-1} in composites with Ag oxide and Ag NPs interfaces, respectively, at a 3 T applied magnetic field. From the MCE measurements, it can be concluded that the magnetocaloric properties of the LBMO compound are enhanced with different sizes of Ni and Ag interfaces at the same temperature range.

4. Conclusions

The effect of Ni and Ag interface size on the transport, magnetoresistive, magnetic and magnetocaloric properties of LBMO compound was investigated. The interaction lack between the interfaces and the LBMO compound suggested the interfaces segregation at LBMO GBs, which increases the GBs' resistance according to the interface size. The increase in GBs' resistance interrupts conduction between grains, which appears as an increase in the resistivity. However, this increases the spin tunnelling effect which leads to the LFMR. For example, the room temperature LFMR of the LBMO compound is enhanced from −1.23% to −4.35, −5.25 and −7.9% with the addition of Ni powder, Ag NPs and Ag oxide interfaces, respectively. The magnetic measurements show a constant T_c value of the LBMO compound with all introduced interfaces (except Ni NWs) due to the complete interaction lack. Whereas, in the Ni NWs-doped composite, the T_c value decreases by 6 K to 342 K as a result of the incomplete interaction lack in this composite. The MCE properties are found to be sensitive to the interface size; the RCP value of the LBMO compound is improved from 44 J kg^{-1} to 107, 167, 92 and 94 J kg^{-1} with the addition of Ni powder, Ni NWs, Ag oxide and Ag NPs interfaces, respectively, at a 3 T applied magnetic field.

Acknowledgements

This work was financially supported by the Spanish MINECO Ref. MAT201347231-C2-1-P, MAT2013-48054-C2-2-R, and the Asturias Government Ref. FC-15-GRUPIN14-085 research projects. The authors would also like to acknowledge the Egyptian Ministry of Higher Education.

References

1 H. Hwang, S. W. Cheong, N. P. Ong and B. Batlogg, *Phys. Rev. Lett.*, 1996, **77**, 2041.
2 S. P. Issac, N. D. Mathur, J. E. Evetts and M. G. Blamire, *Appl. Phys. Lett.*, 1998, **72**, 2038.
3 A. M. Ahmed, H. F. Mohamed, A. K. Diab, A. A. Mohamed, A. E. A. Mazen and A. M. Mohamed, *Indian J. Phys.*, 2015, **89**, 561.
4 L. W. Lei, Z. Y. Fu, J. Y. Zhang and H. Wang, *Mater. Sci. Eng., B*, 2006, **128**, 70.
5 Y. Lu, X. W. Li, G. Q. Gong, G. Xiao, A. Gupta, P. Lecoeur, J. Z. Sun, Y. Y. Wang and V. P. Dravid, *Phys. Rev. B: Condens. Matter*, 1996, **54**, R8357.
6 J. C. Debnath, R. Zeng, J. H. Kim and S. X. Dou, *J. Appl. Phys.*, 2010, **107**, 09A916.
7 D. K. Petrov, L. K. Elbaun, J. Z. Sun, C. Field and P. R. Duncombe, *Appl. Phys. Lett.*, 1999, **75**, 995.
8 Z. C. Xia, S. L. Yuan, W. Feng, L. J. Zhang, G. H. Zhang, J. Tang, L. Liu, S. Liu, G. Peng, D. W. Niu, L. Chen, Q. H. Zheng, Z. H. Fang and C. Q. Tang, *Solid State Commun.*, 2003, **128**, 291.
9 S. Valencia, O. Castano, J. Fontcuberta, B. Martinez and L. Balcells, *J. Appl. Phys.*, 2003, **94**, 2524.
10 A. A. Mohamed, V. Vega, M. Ipatov, A. M. Ahmed and B. Hernando, *J. Alloys Compd.*, 2016, **657**, 495.
11 A. A. Mohamed, V. Vega, M. Ipatov, A. M. Ahmed and B. Hernando, *J. Alloys Compd.*, 2016, **665**, 394.
12 D. Alberts, V. Vega, R. Pereiro, N. Bordel, V. M. Prida, A. Bengtson and A. S. Medel, *Anal. Bioanal. Chem.*, 2010, **396**, 2833.
13 M. A. Mohamed, *International Journal of Nanomaterials and Chemistry*, 2015, **1**, 103.
14 C. V. Vazquez, M. C. Blanco, M. A. L. Quintela, R. D. Sanchez, J. Rivas and S. B. Oseroff, *J. Mater. Chem.*, 1998, **8**, 991.
15 C. Zener, *Phys. Rev.*, 1951, **81**, 440.
16 A. de Andres, M. G. Hernandez and J. L. Martinez, *Phys. Rev. B: Condens. Matter*, 1999, **60**, 7328.

17 S. Karmakar, S. Taran, B. K. Chaudhuri, H. Sakata, C. P. Sun, C. L. Huang and H. D. Yang, *J. Phys. D: Appl. Phys.*, 2005, **38**, 3757.
18 Z. Sheng, Y. Sun, X. Zhu, W. Song and P. Yan, *J. Phys. D: Appl. Phys.*, 2007, **40**, 3300.
19 S. Gupta, R. Ranjit, C. Mitra, P. Raychaudhuri and R. Pinto, *Appl. Phys. Lett.*, 2001, **78**, 362.
20 W. J. Lu, Y. P. Sun, X. B. Zhu, W. H. Song and J. J. Du, *Mater. Lett.*, 2006, **60**, 3207.
21 T. F. Zhou, G. Li, N. Y. Wang, B. M. Wang, X. G. Li and Y. Chen, *Appl. Phys. Lett.*, 2006, **88**, 232508.
22 H. J. Kim and S. I. Yoo, *J. Alloys Compd.*, 2012, **521**, 30.
23 L. Yan, L. B. Kong, T. Yang, W. C. Goh, C. Y. Tan, C. K. Ong, M. A. Rahman, T. Osipowicz and M. Q. Ren, *J. Appl. Phys.*, 2004, **96**, 1568.
24 A. Arrott, *Phys. Rev.*, 1957, **108**, 1394.
25 S. K. Banerjee, *Phys. Lett.*, 1964, **12**, 16.
26 V. K. Pecharsky and K. A. Gschneidner Jr, *J. Appl. Phys.*, 1999, **86**, 565.
27 M. H. Phan and S. C. Yu, *J. Magn. Magn. Mater.*, 2007, **308**, 325.
28 M. Pekala, K. Pekala, V. Drozd, J. F. Fagnard and P. Vanderbemden, *J. Alloys Compd.*, 2015, **629**, 98.